NACA RM E51K05

NACA

RESEARCH MEMORANDUM

INFLUENCE OF FUSELAGE AND CANARD-TYPE CONTROL SURFACE ON THE FLOW FIELD ADJACENT TO A REARWARD FUSELAGE STATION AT A MACH NUMBER OF 2.0 - DATA PRESENTATION

By Evan A. Fradenburgh, Leonard J. Obery and John F. Mello

Lewis Flight Propulsion Laboratory
Cleveland, Ohio

NATIONAL ADVISORY COMMITTEE FOR AERONAUTICS

WASHINGTON

January 21, 1952

NATIONAL ADVISORY COMMITTEE FOR AERONAUTICS

RESEARCH MEMORANDUM

INFLUENCE OF FUSELAGE AND CANARD-TYPE CONTROL SURFACE ON THE FLOW FIELD ADJACENT TO A REARWARD FUSELAGE STATION AT A MACH NUMBER OF 2.0 - DATA PRESENTATION

By Evan A. Fradenburgh, Leonard J. Obery

and John F. Mello

SUMMARY

Measurements of the local total pressures and flow-deflection angles in the flow field of a body and a canard-type control-surface combination were made at a rearward fuselage station (69 percent of the body length downstream of the nose) which corresponded to a possible engine inlet location. Data are presented for a Mach number of 2.0, body angles of attack from 0° to 6°, and control-surface deflection angles from 0° to $9\frac{1}{2}^\circ$.

The survey showed large total-pressure losses in the wake of the control surface and a pronounced shift in the circumferential distribution of the boundary-layer air about the fuselage due to deflection of the control surface. On a canard-type supersonic aircraft configuration, a rearward location of an engine inlet, either on the body surface or in the stream adjacent to the body, must therefore be carefully selected for optimum engine performance.

INTRODUCTION

Disturbances originated by the longitudinal control surface in a canard or "tail-first" type aircraft are propagated downstream and appear as losses in total pressure in the control-surface wake and flow angularity because of the trailing vortices. If an air inlet is located in the disturbed region, the efficiency of the propulsion system may be impaired.

An experimental investigation to determine the influence of a fuselage and canard-type control-surface combination on the flow field

approximately 10 mean geometric chords downstream of the control surface was conducted in the NACA Lewis 8- by 6-foot supersonic wind tunnel. Downwash and sidewash angles and total pressures in the flow field were measured in the investigation. Data are presented for a Mach number of 2.0, body angles of attack from 0° to 6°, and control-surface deflection angles from 0° to $9\frac{1}{2}^\circ$. The Reynolds number in this investigation was approximately 2.7×10^6 based on the mean geometric chord of the control surface.

SYMBOLS

The following symbols are used in this report:

P	total pressure
d	diameter
x	distance from fuselage nose
δ_c	control-surface deflection angle measured from body center line and positive when trailing edge is down

Subscripts:

0	free stream
1	survey station

APPARATUS AND PROCEDURE

A sketch of the model and supporting strut is shown in figure 1. A body of revolution having a maximum diameter of 9 inches and a length-diameter ratio of 12 was combined with a control surface having a plan area of 135 square inches, an aspect ratio of 3.0, a taper ratio of 0.5, and an unswept 50-percent chord line. The airfoil section was a double circular arc, 5-percent thick except near the root where the thickness ratio was gradually increased to 8 percent for strength.

The all-movable control surface was hinged about its 50-percent chord line and was remotely operated. The nose portion of the body adjacent to the forward half of the control surface was fixed to and deflected with the surface.

A sketch of the survey apparatus is shown in figure 2. The survey station, 74.1 inches downstream of the nose of the body, was 9.8 mean geometric chord lengths downstream of the 50-percent chord line of the control surface. The wedges in the survey apparatus were used to measure local Mach numbers and flow deflection angles; two-dimensional flow theory was assumed for the calculations. The local Mach numbers were used to correct the pressures measured with the survey pitot tubes for normal shock losses. Duplicate runs were made with the survey apparatus shifted spanwise, as shown in figure 2, to provide surveys every $2\frac{1}{2}$ inches. The wedge survey rakes were canted downward 5° with respect to the body centerline so that the wedges, which are limited in their useful angle of attack range, would operate from -5° to 5° as the body angle of attack was varied from 0° to 10°. The downwash and sidewash components of the flow deflection were measured with the horizontal and vertical wedges, respectively, on opposite sides of the body. The total-pressure ratios obtained in the manner described have an estimated accuracy of ± 0.02 at points of measurement. The maximum error in the downwash and sidewash measurements is estimated to be 0.5°.

Four boundary-layer rakes were used in the survey at 45°, 90°, 135°, and 180° from the top of the body. As the model support strut prevented placing a rake on the top of the body at the survey plane, the boundary-layer survey was completed with the lower rakes by running the body and control surface at negative angles. The pressures measured with the boundary-layer rakes were corrected for shock losses by assuming that the static pressure varied linearly from the measured value at the base of the rake to free-stream static pressure at the tip. This assumption resulted in the most reasonable boundary-layer profiles for the body alone and consequently was used for all model conditions. Although some error may be involved, the indicated effects of the control-surface deflection on the boundary layer are considered qualitatively valid.

Photographs of the model and survey apparatus are shown in figures 3 and 4.

PRESENTATION OF DATA

The results of the investigation are presented in figures 5 to 7 for the body alone and in figures 8 to 10 for the body and control surface. The data are presented as contours of the ratio of the local total pressure P_1 to the free-stream total pressure P_0, and as vector plots of the local flow-deflection angles with respect to the free-stream direction. In these vector plots, the length of a vector is proportional to the magnitude of the angle between the local flow and the free-stream

direction. The horizontal and vertical components of the vector represent, respectively, the sidewash and downwash angles. The semicircles on the plots represent the fuselage cross section at the survey plane and the dashed straight line in figures 8 to 10 represents the trailing edge of the control surface projected to the survey plane in the free-stream direction. For cases where one component of the flow deflection was not obtained, the measured component is shown as a dashed line on the vector plots.

Measurements obtained for the body without the control surface at 0° angle of attack are presented in figure 5. Although some irregularity is apparent in the flow deflection angles shown because of errors in alining the wedges, a downwash is evident near the body. This downwash is due to the model support strut, which caused a high static-pressure field near the top of the body. This effect is also evidenced in figure 8(a) as a slight downward displacement of the wake from the control surface. In order to minimize the effect of the support strut on the flow angularity and to eliminate wedge alinement errors, the deflection angles measured for the body alone at 0° angle of attack (data of figure 5) were subtracted from the measured values for all other model conditions presented.

The effect of the model support strut on the total pressures in the survey field was negligible. The Mach number distribution was influenced considerably by the strut, however, and is not presented as it is not generally representative of the flow field.

The model configuration was also investigated at Mach number 1.8; however, the results were generally the same as those shown for a Mach number of 2.0 and no data are presented. The losses in total pressure were slightly lower at Mach number 1.8 than at 2.0.

CONCLUDING REMARKS

The results of the investigation indicate that regions of large total-pressure loss and flow angularity exist as far rearward as 10 mean geometric chord lengths downstream of a canard-type control surface. Furthermore, when the control surface provides lift, the circumferential distribution of the boundary-layer air around the fuselage is distorted from the pattern measured for the body without a control surface. Therefore, care must be exercised in locating fuselage inlets or engine nacelles downstream of a canard-type control surface if serious penalties in performance are to be avoided.

Lewis Flight Propulsion Laboratory
National Advisory Committee for Aeronautics
Cleveland, Ohio.

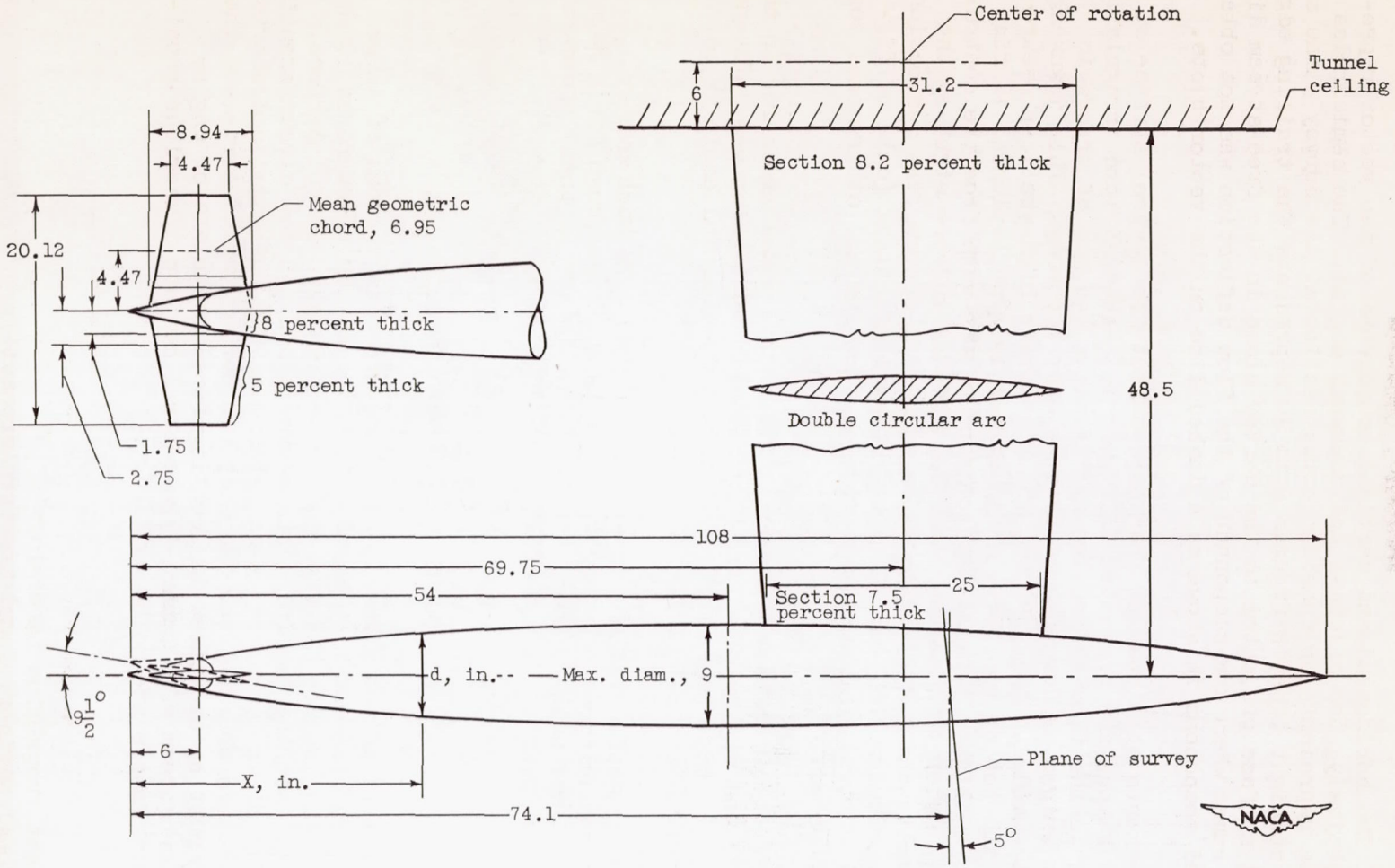

Figure 1. - Sketch of model and supporting strut. Body defined by $d = 9\left[1 - \left(1 - \frac{X}{54}\right)^2\right]^{\frac{3}{4}}$, inches.

(All dimensions in inches.)

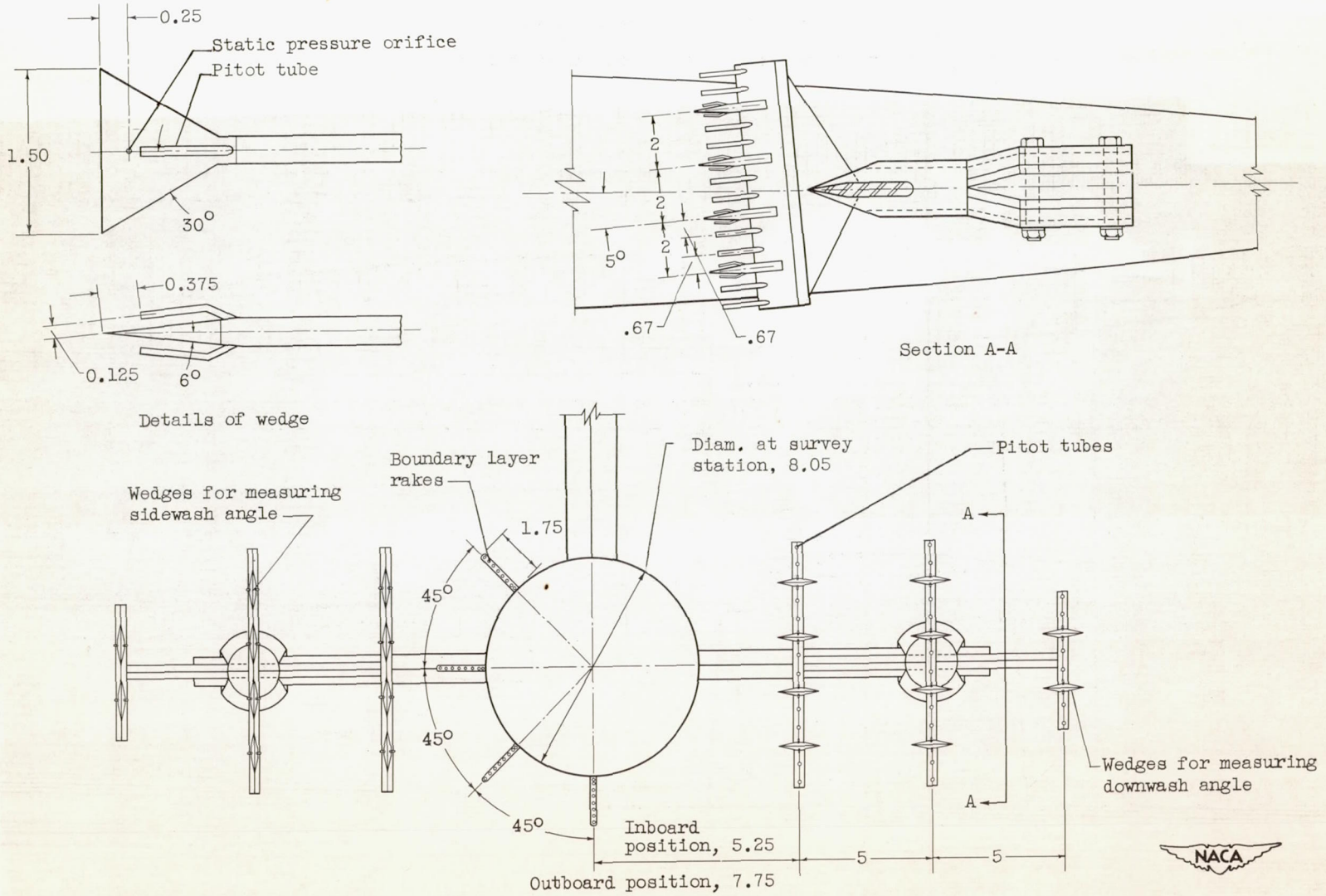

Figure 2. - Sketch of survey apparatus. (All dimensions in inches.)

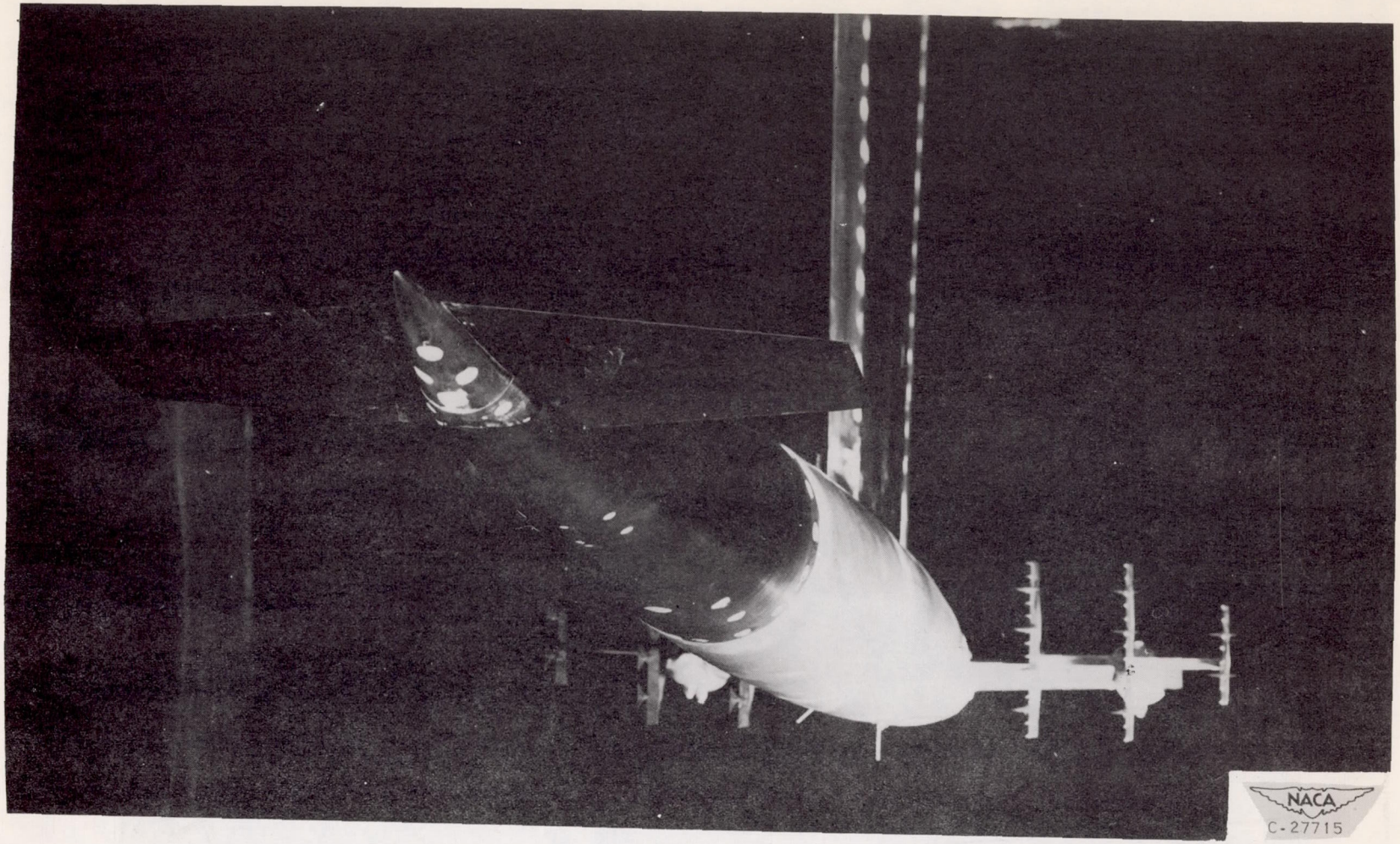

Figure 3. - Fuselage-control surface survey model installed in tunnel. Angle of attack, 10°; control-surface deflection angle, $9\frac{1}{2}^{\circ}$.

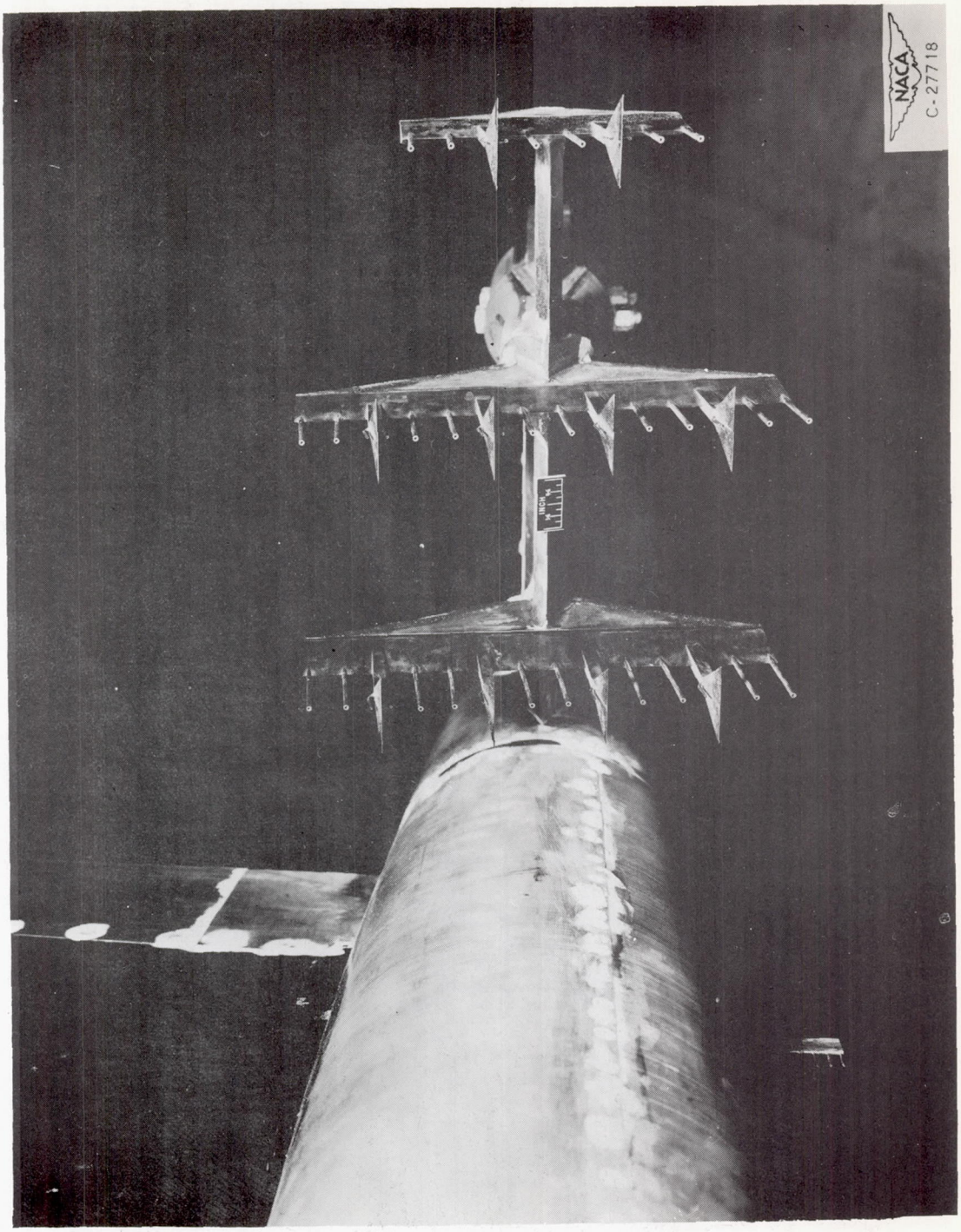

Figure 4. - Wake-survey apparatus in inboard position.

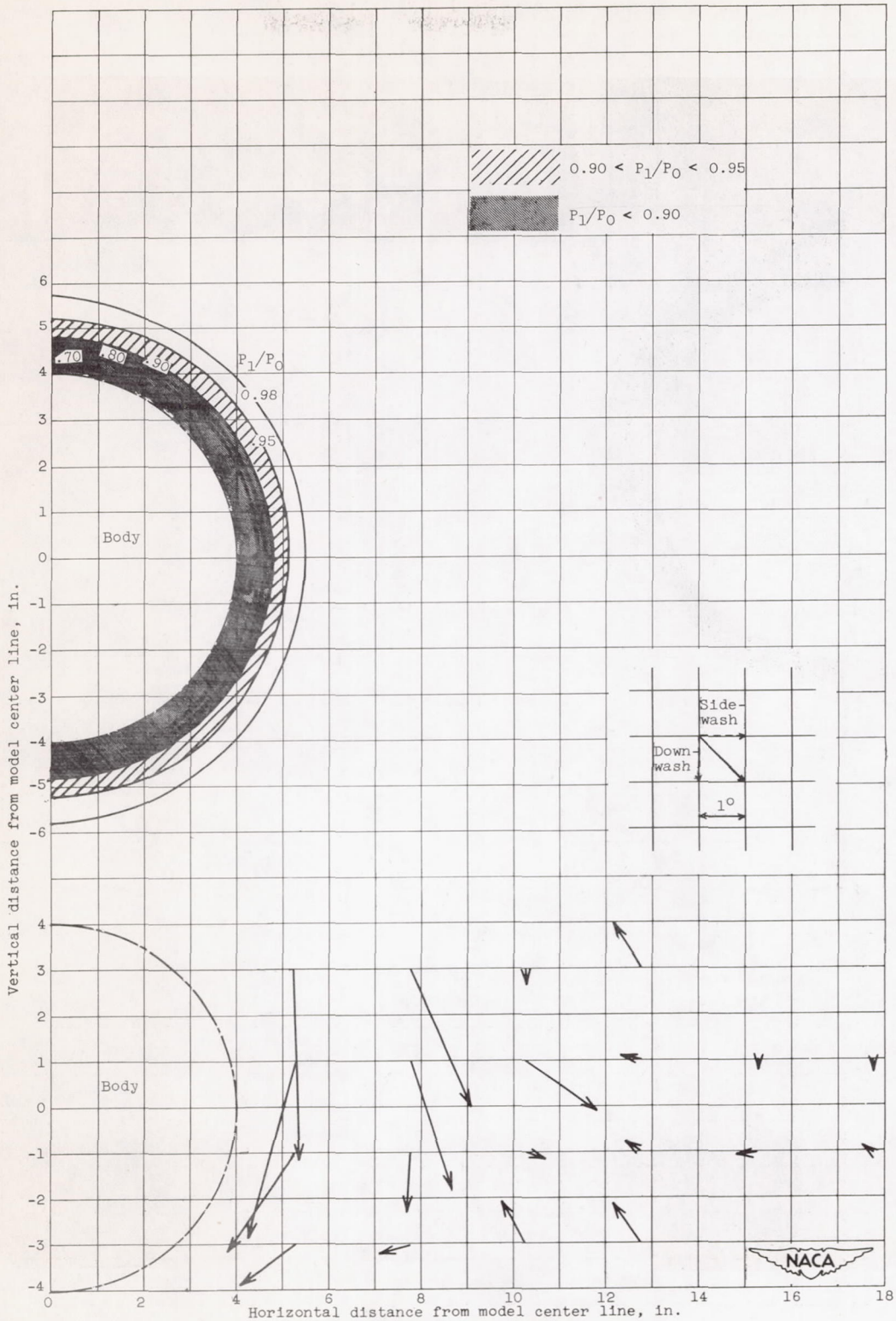

Figure 5. - Total-pressure-ratio contours and flow-deflection angles of flow for body without control surface. Angle of attack, 0°. (Flow deflection vectors not corrected for wedge misalinement or for support strut interference.)

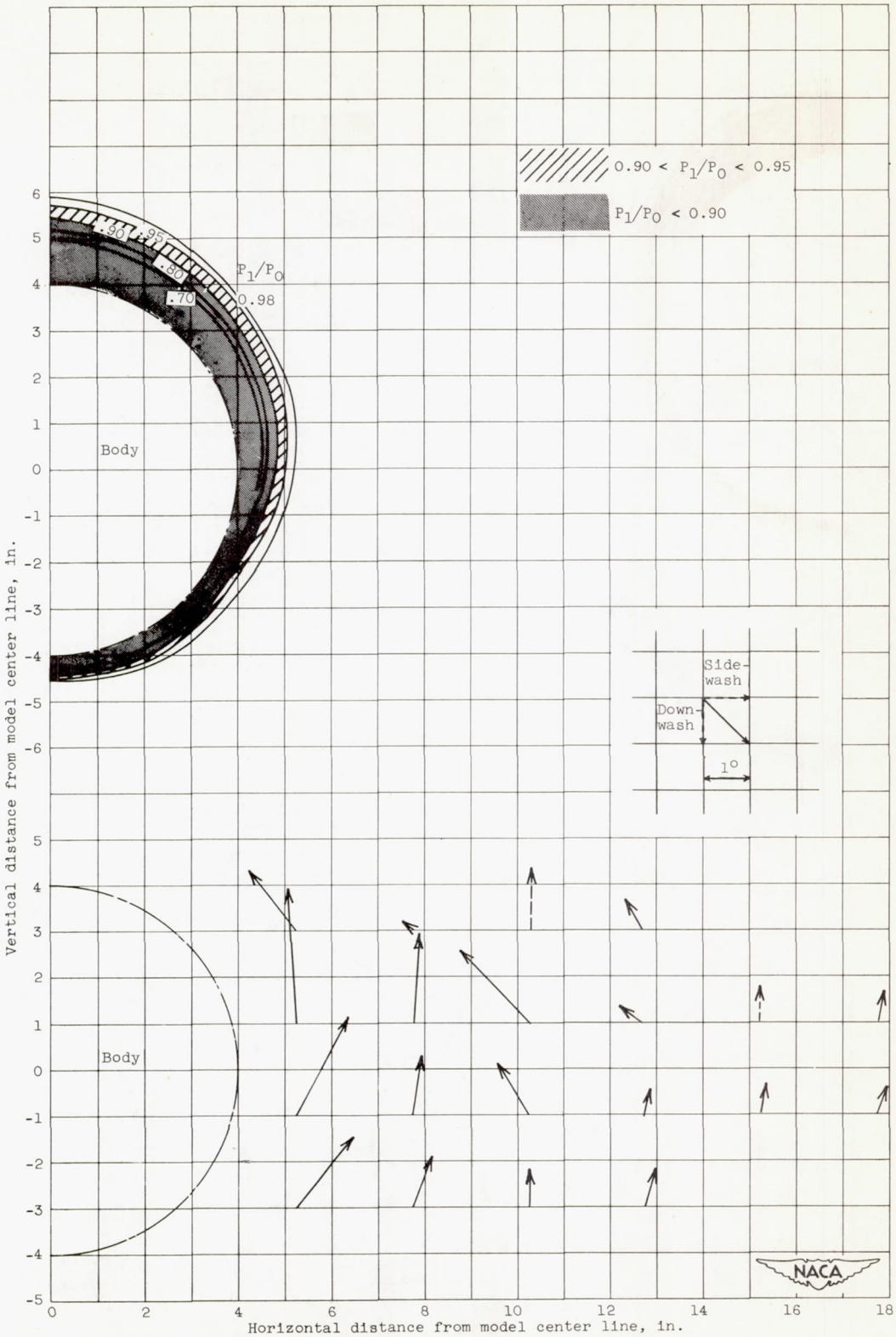

Figure 6. - Total-pressure-ratio contours and flow-deflection angles of flow for body without control surface. Angle of attack, 3°.

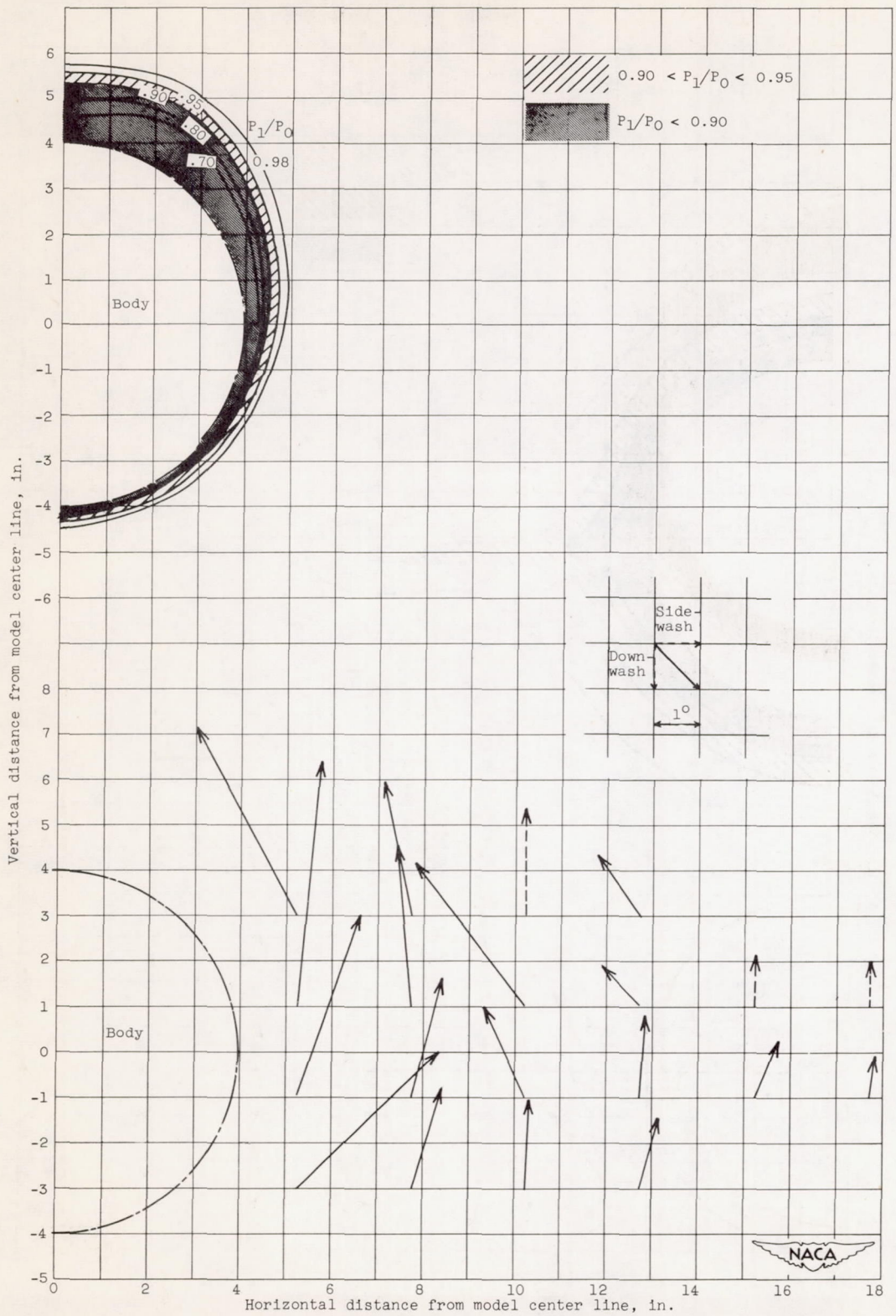

Figure 7. - Total-pressure-ratio contours and flow-deflection angles of flow for body without control surface. Angle of attack, 6°.

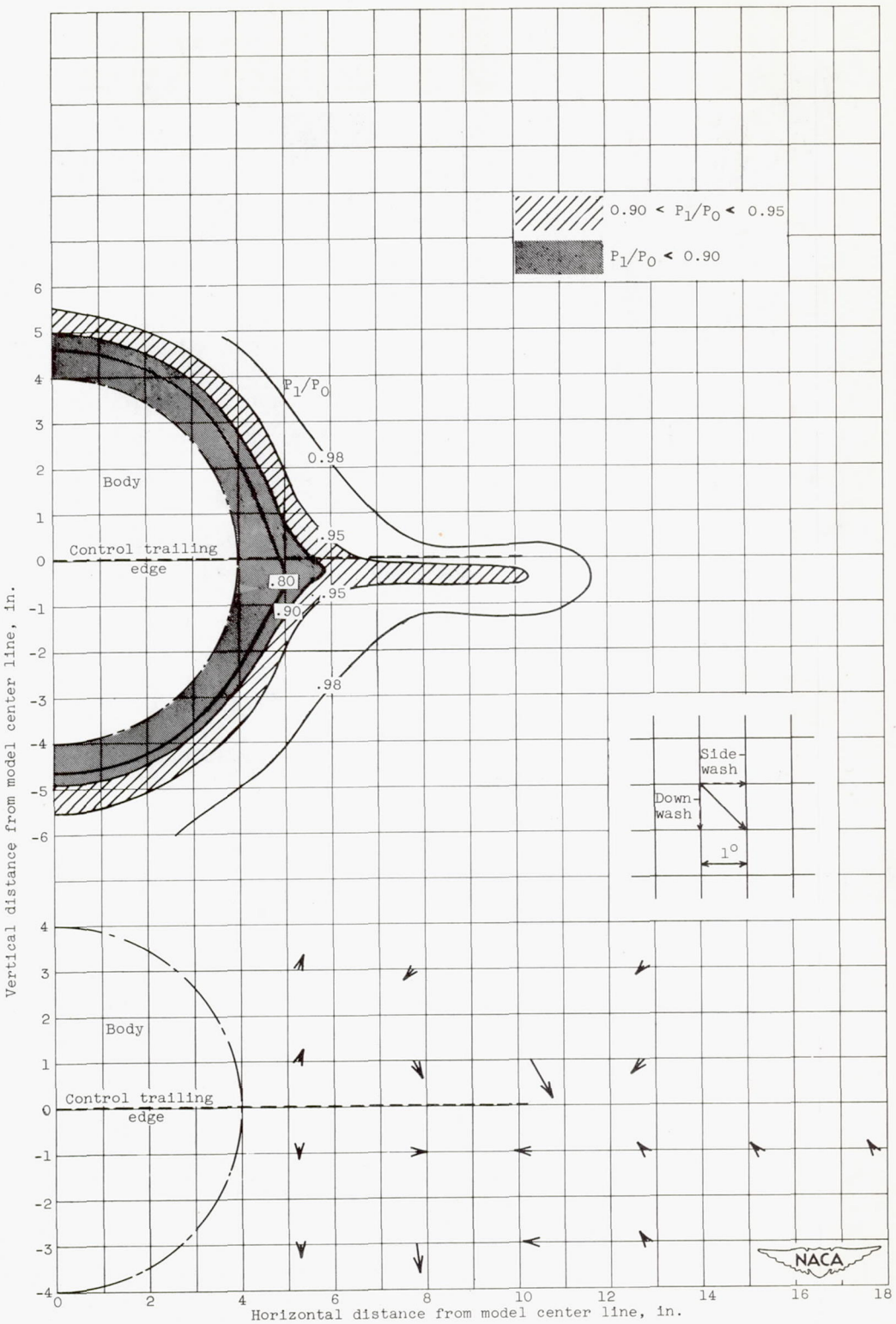

(a) $\delta_c = 0^\circ$.

Figure 8. - Total-pressure-ratio contours and flow-deflection angles of flow for body with control surface. Angle of attack, 0°.

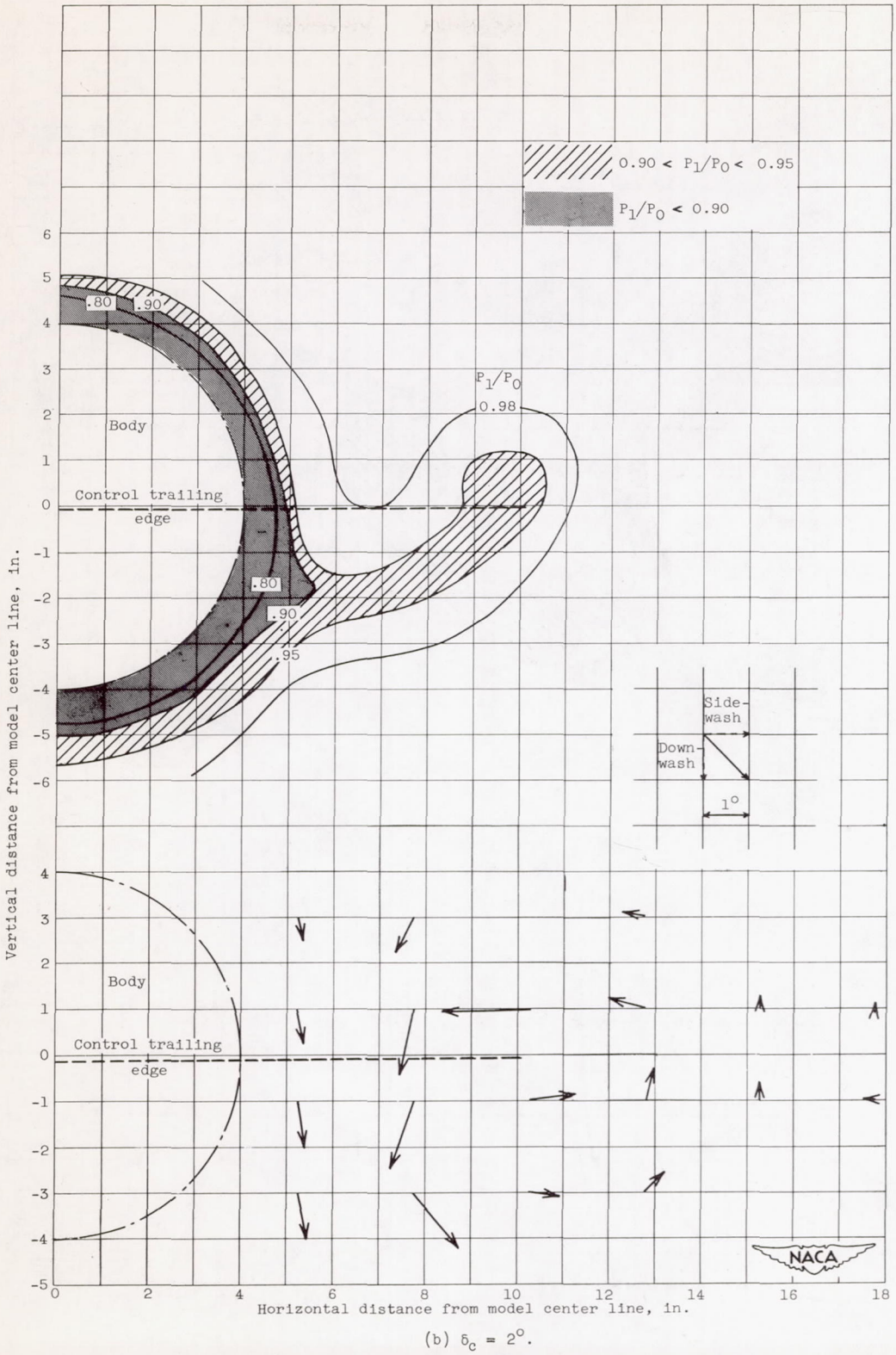

(b) $\delta_c = 2^\circ$.

Figure 8. - Continued. Total-pressure-ratio contours and flow-deflection angles of flow for body with control surface. Angle of attack, 0°.

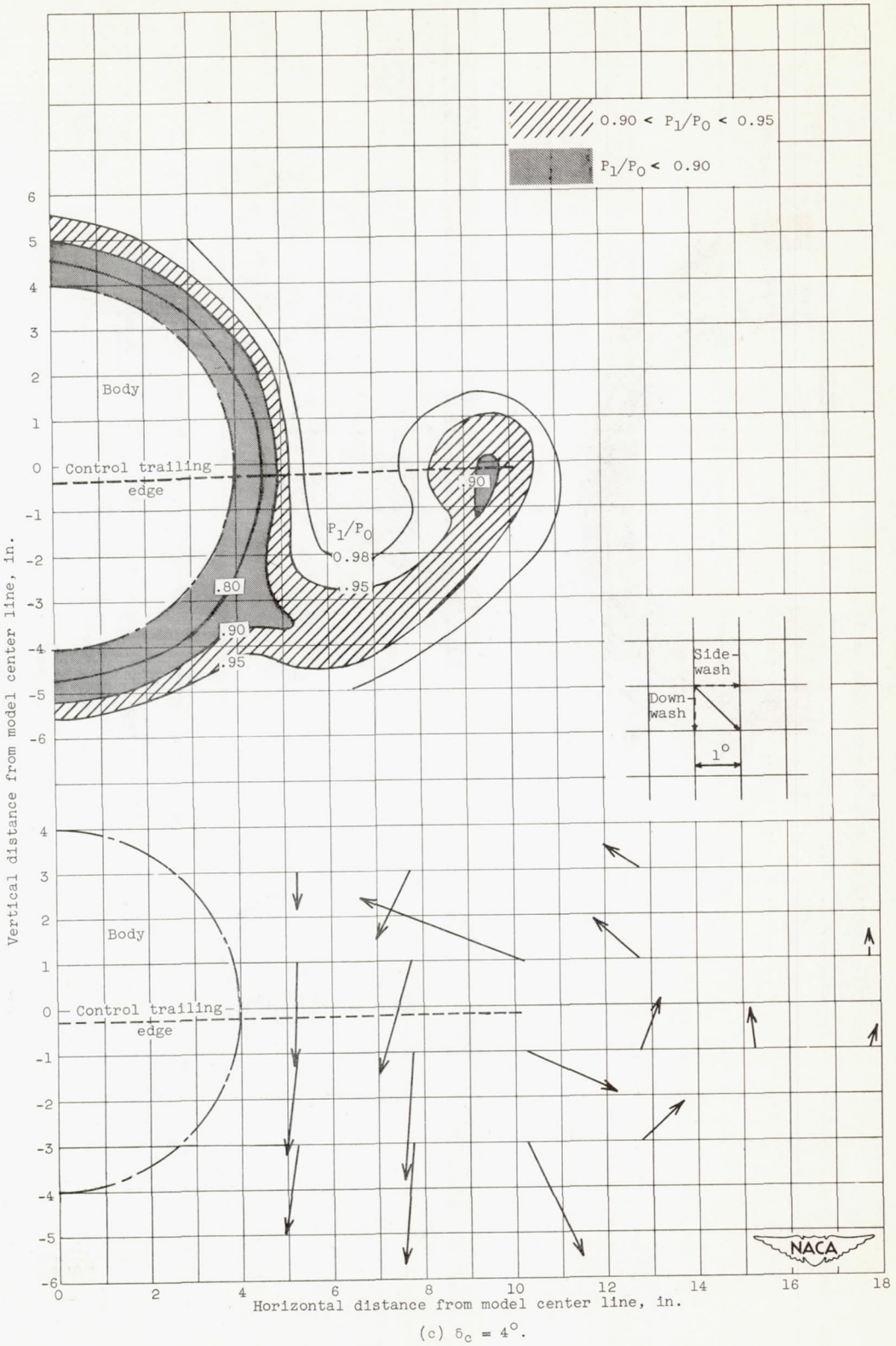

(c) $\delta_c = 4^\circ$.

Figure 8. - Continued. Total-pressure-ratio contours and flow-deflection angles of flow for body with control surface. Angle of attack, 0°.

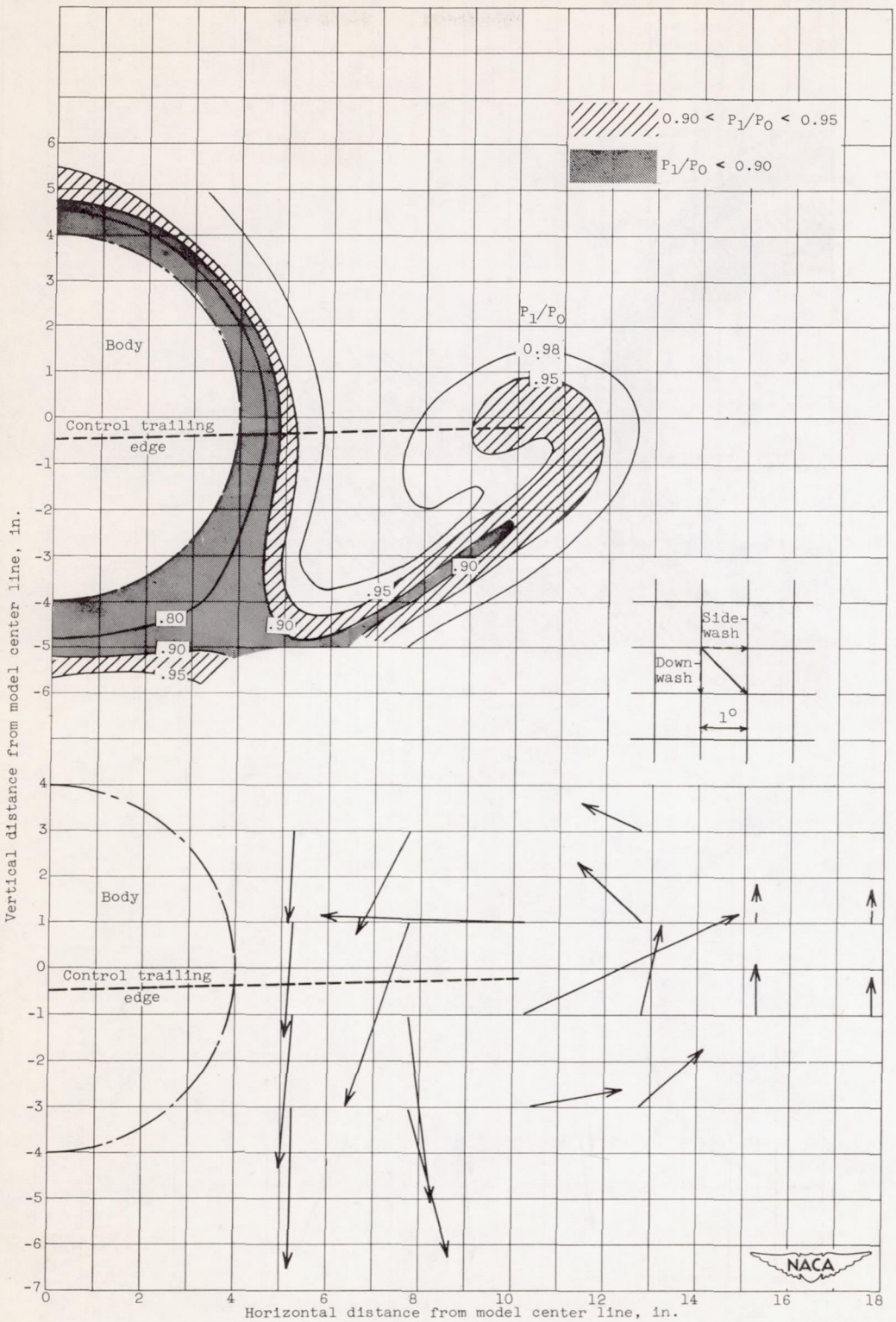

(d) $\delta_c = 6^\circ$.

Figure 8. - Continued. Total-pressure-ratio contours and flow-deflection angles of flow for body with control surface. Angle of attack, 0°.

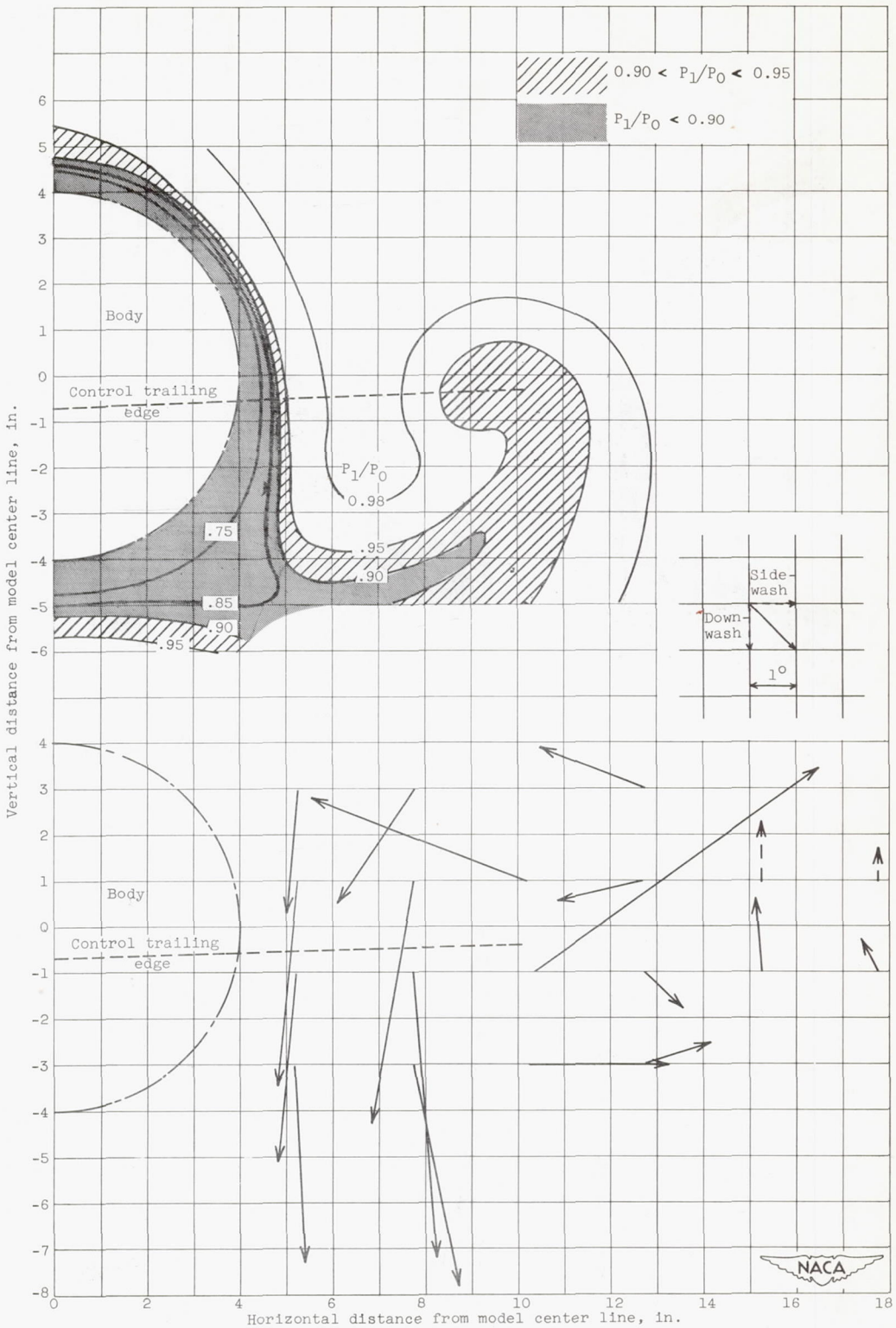

(e) $\delta_c = 8^\circ$.

Figure 8. - Continued. Total-pressure-ratio contours and flow-deflection angles of flow for body with control surface. Angle of attack, 0°.

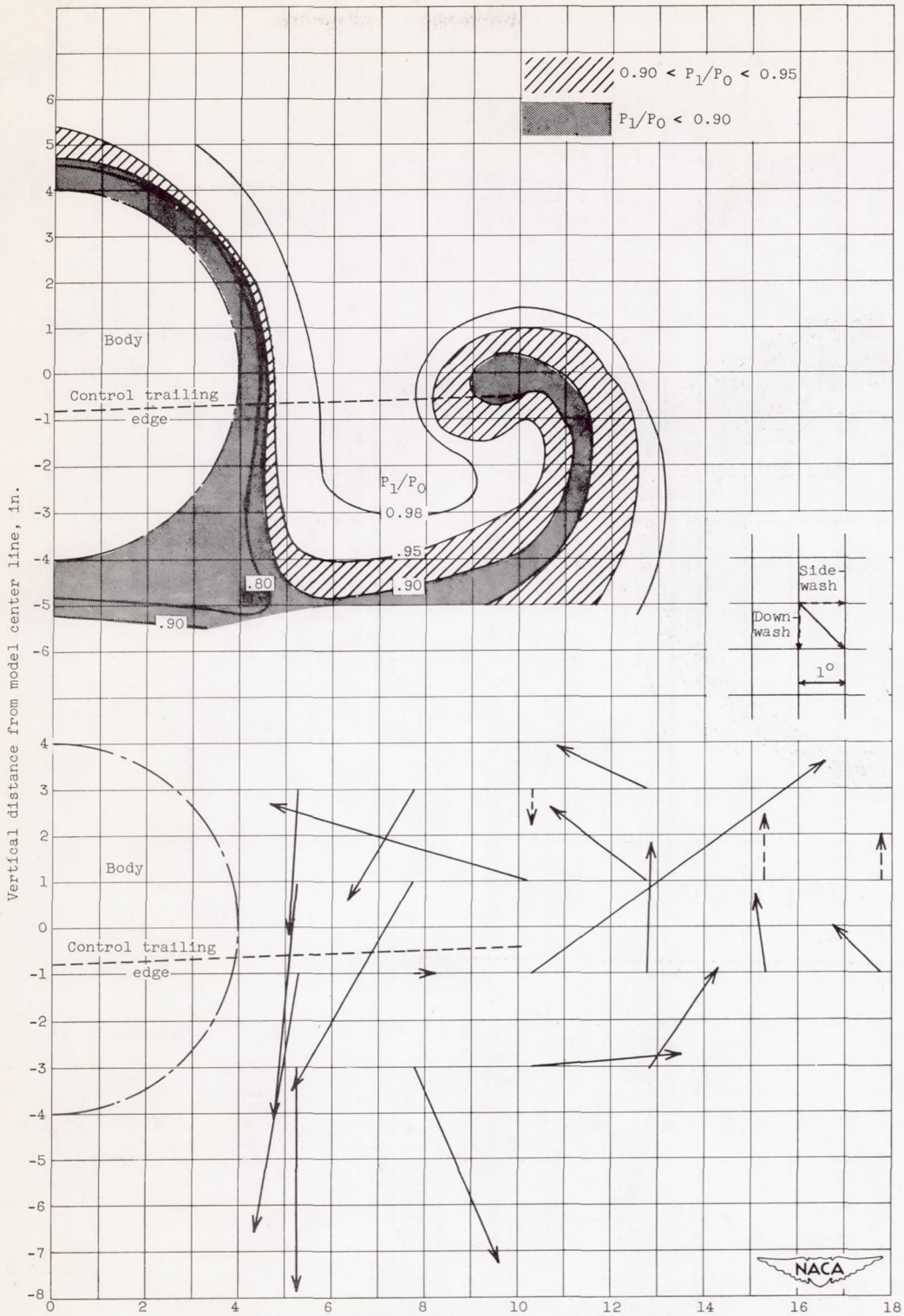

(f) $\delta_c = 9\frac{1}{2}^\circ$.

Figure 8. - Concluded. Total-pressure-ratio contours and flow-deflection angles of flow for body with control surface. Angle of attack, 0°.

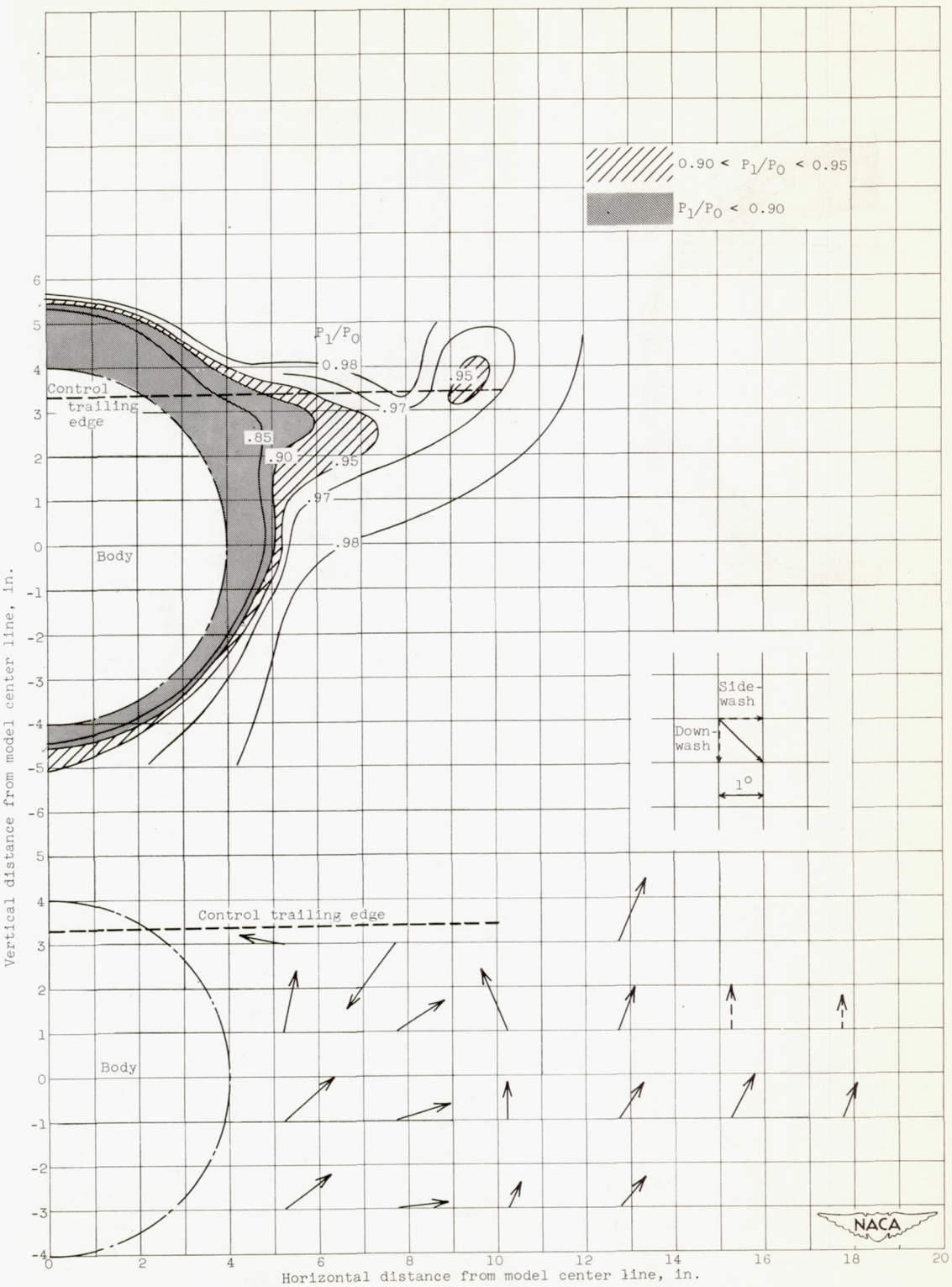

(a) $\delta_c = 0^\circ$.

Figure 9. - Total-pressure-ratio contours and flow-deflection angles of flow for body with control surface. Angle of attack, 3°.

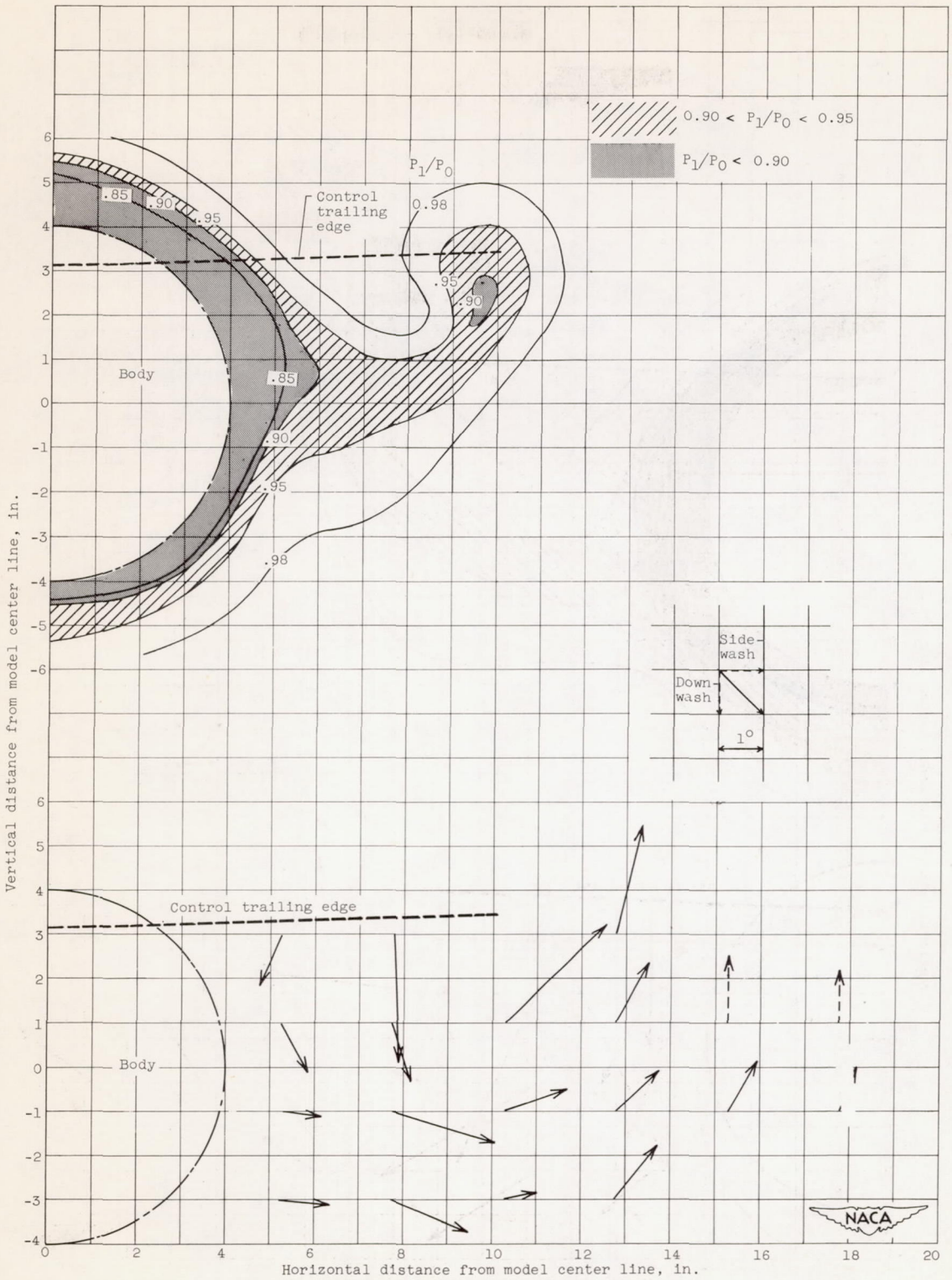

(b) $\delta_c = 3^\circ$.

Figure 9. - Continued. Total-pressure-ratio contours and flow-deflection angles of flow for body with control surface. Angle of attack, 3°.

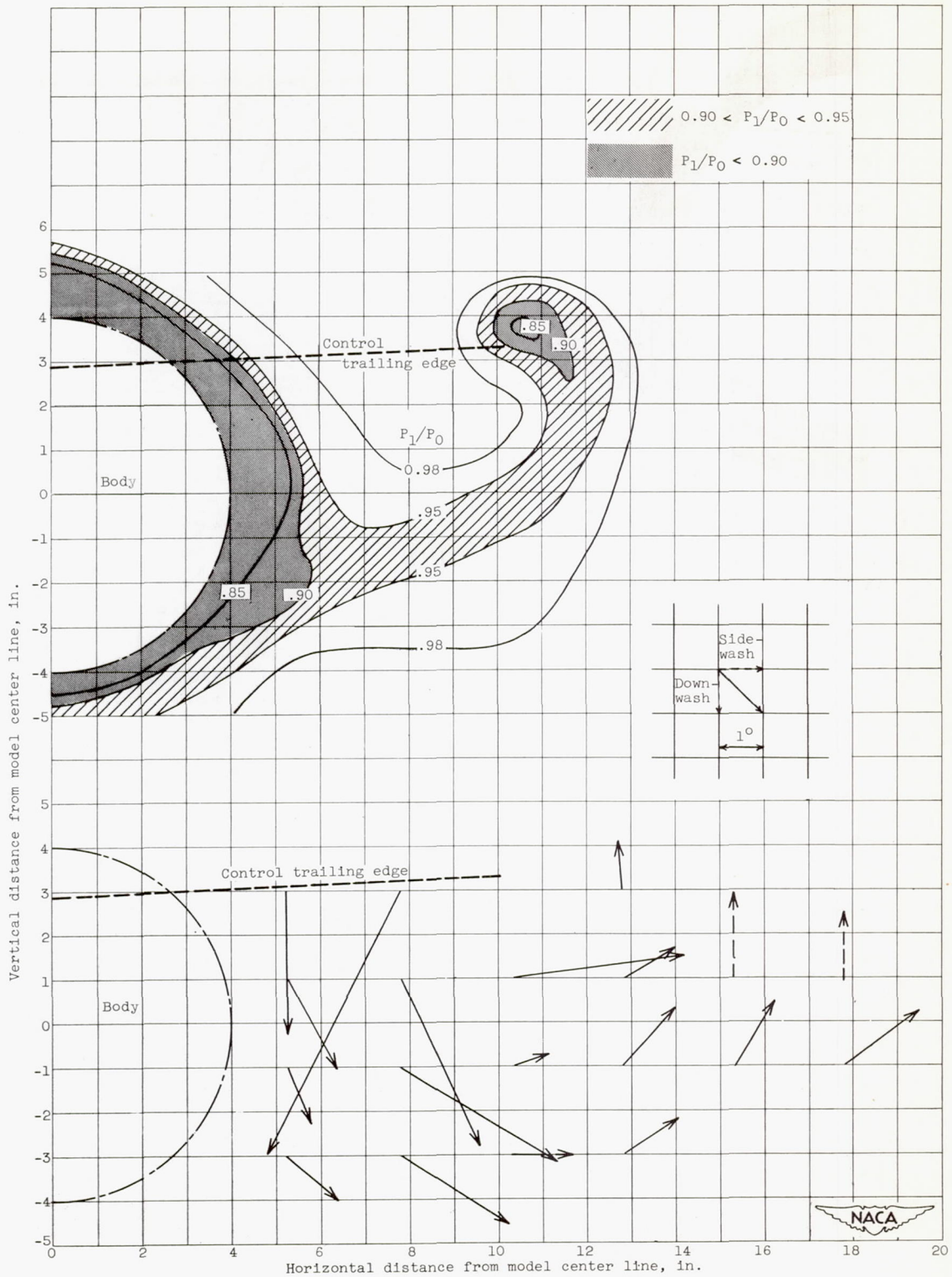

(c) $\delta_c = 6^\circ$.

Figure 9. - Continued. Total-pressure-ratio contours and flow-deflection angles of flow for body with control surface. Angle of attack, 3°.

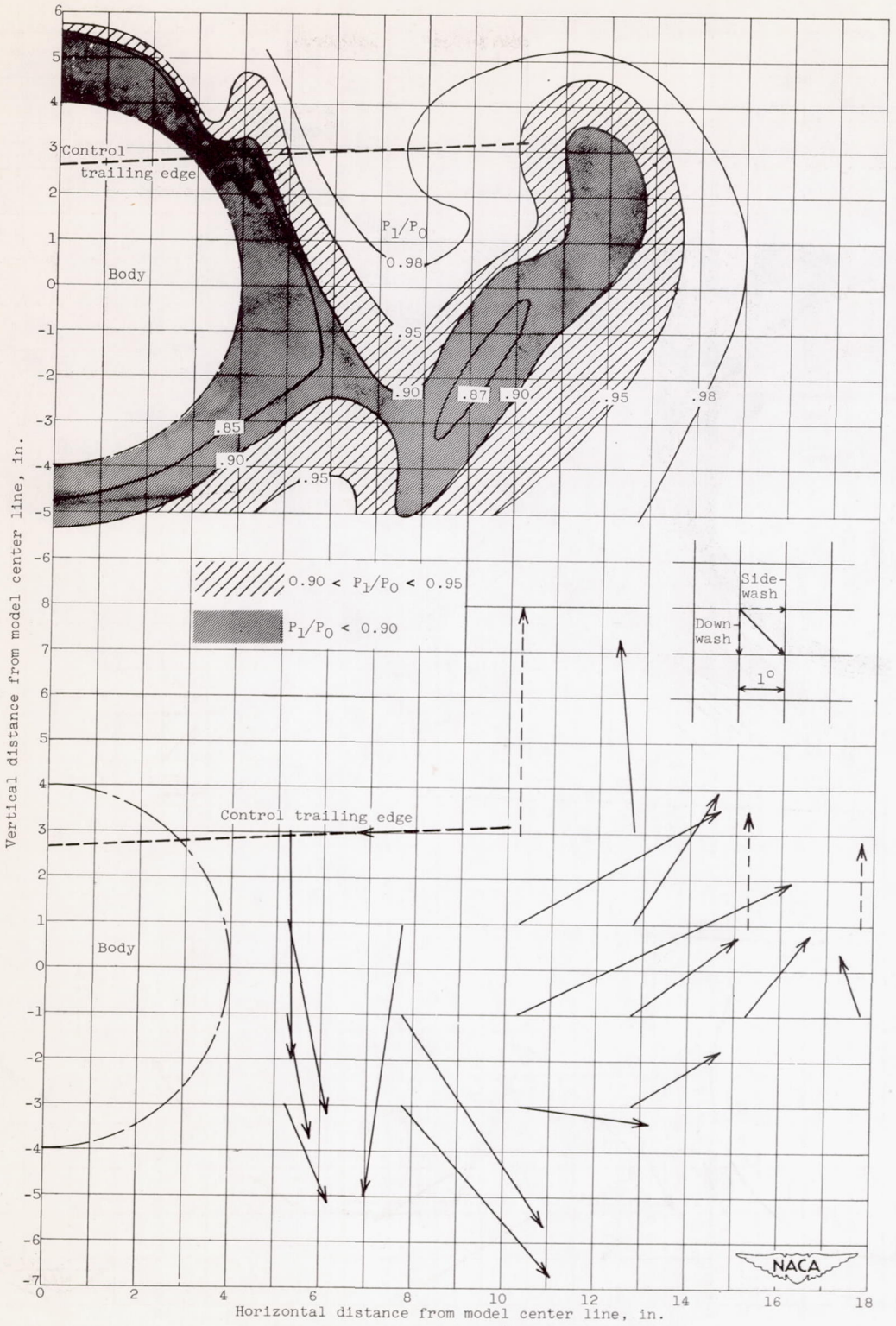

(d) $\delta_c = 9\frac{1}{2}^\circ$.

Figure 9. - Concluded. Total-pressure-ratio contours and flow-deflection angles of flow for body with control surface. Angle of attack, 3°.

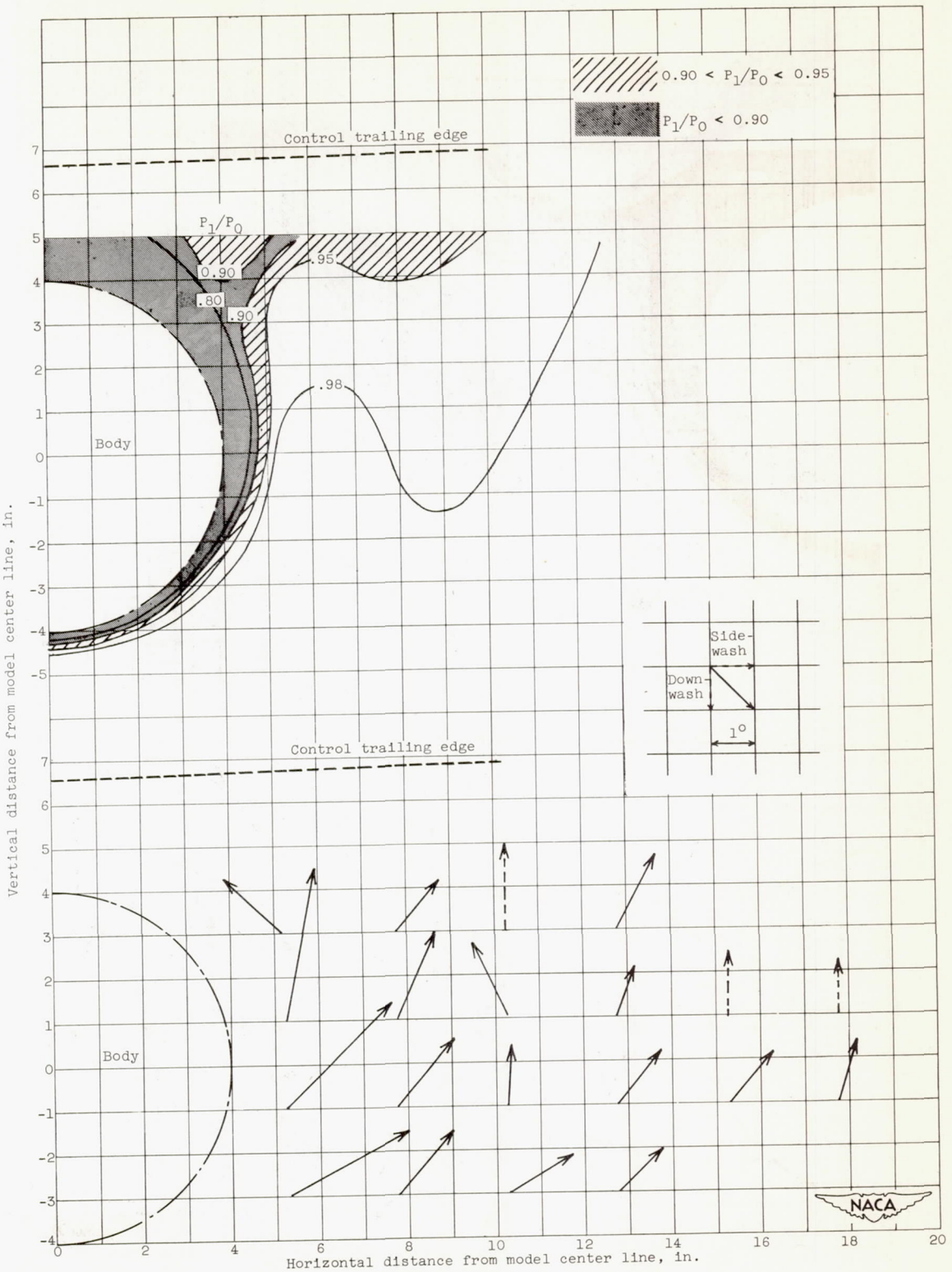

(a) $\delta_c = 0^\circ$.

Figure 10. - Total-pressure-ratio contours and flow-deflection angles of flow for body with control surface. Angle of attack, 6°.

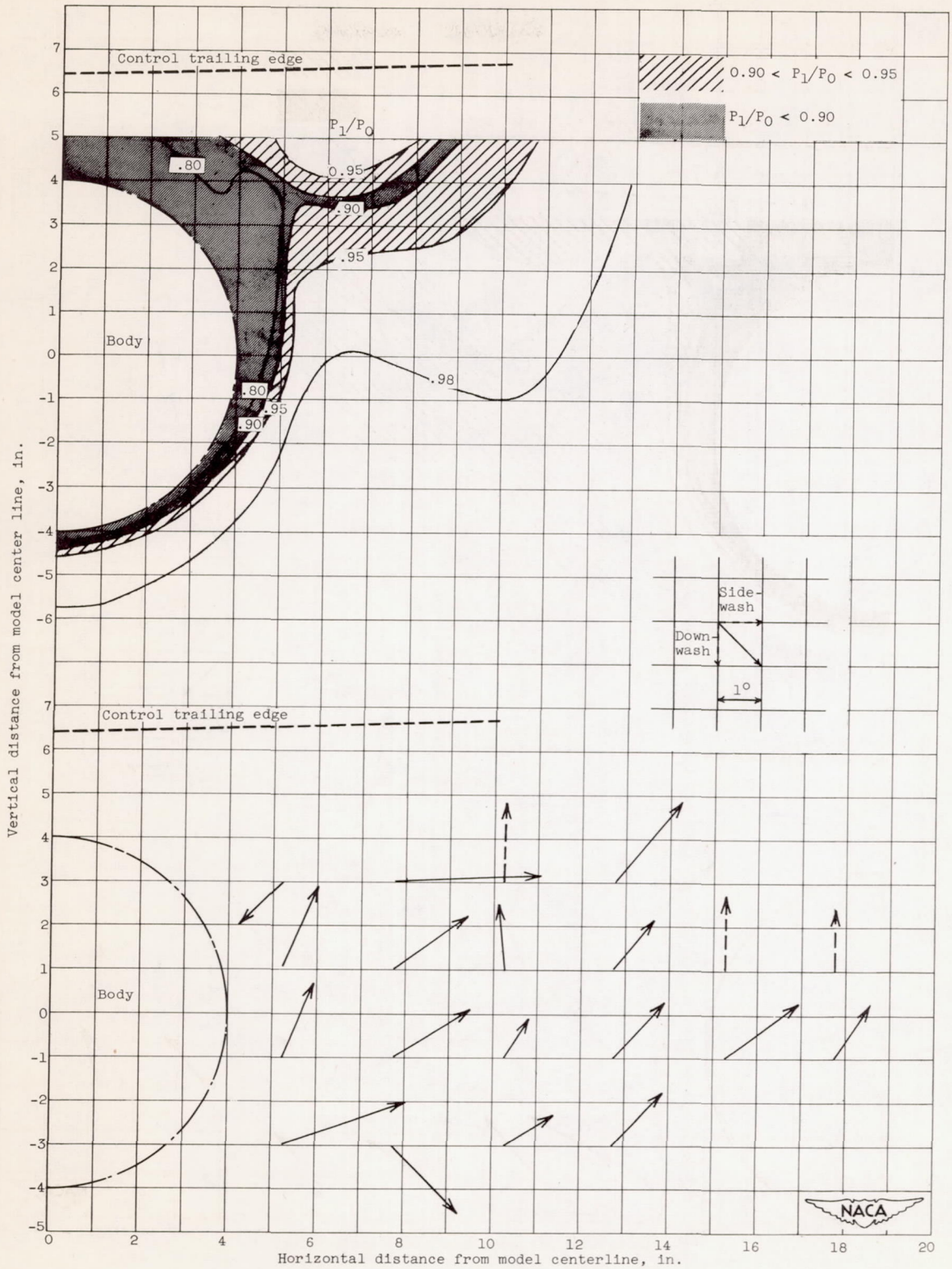

(b) $\delta_c = 3^\circ$.

Figure 10. - Continued. Total-pressure-ratio contours and flow-deflection angles of flow for body with control surface. Angle of attack, 6°.

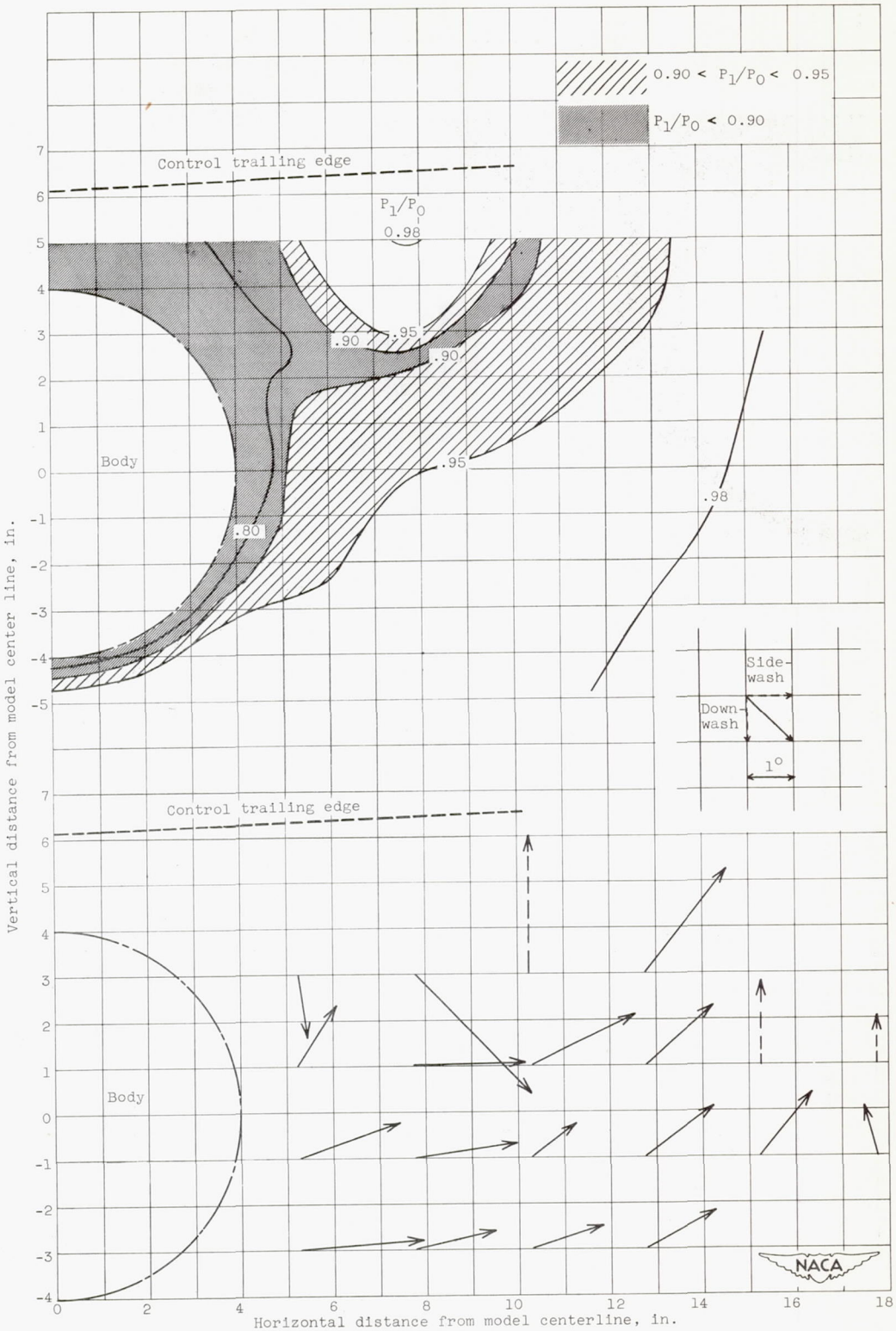

(c) $\delta_c = 6^\circ$.

Figure 10. - Continued. Total-pressure-ratio contours and flow-deflection angles of flow for body with control surface. Angle of attack, 6°.

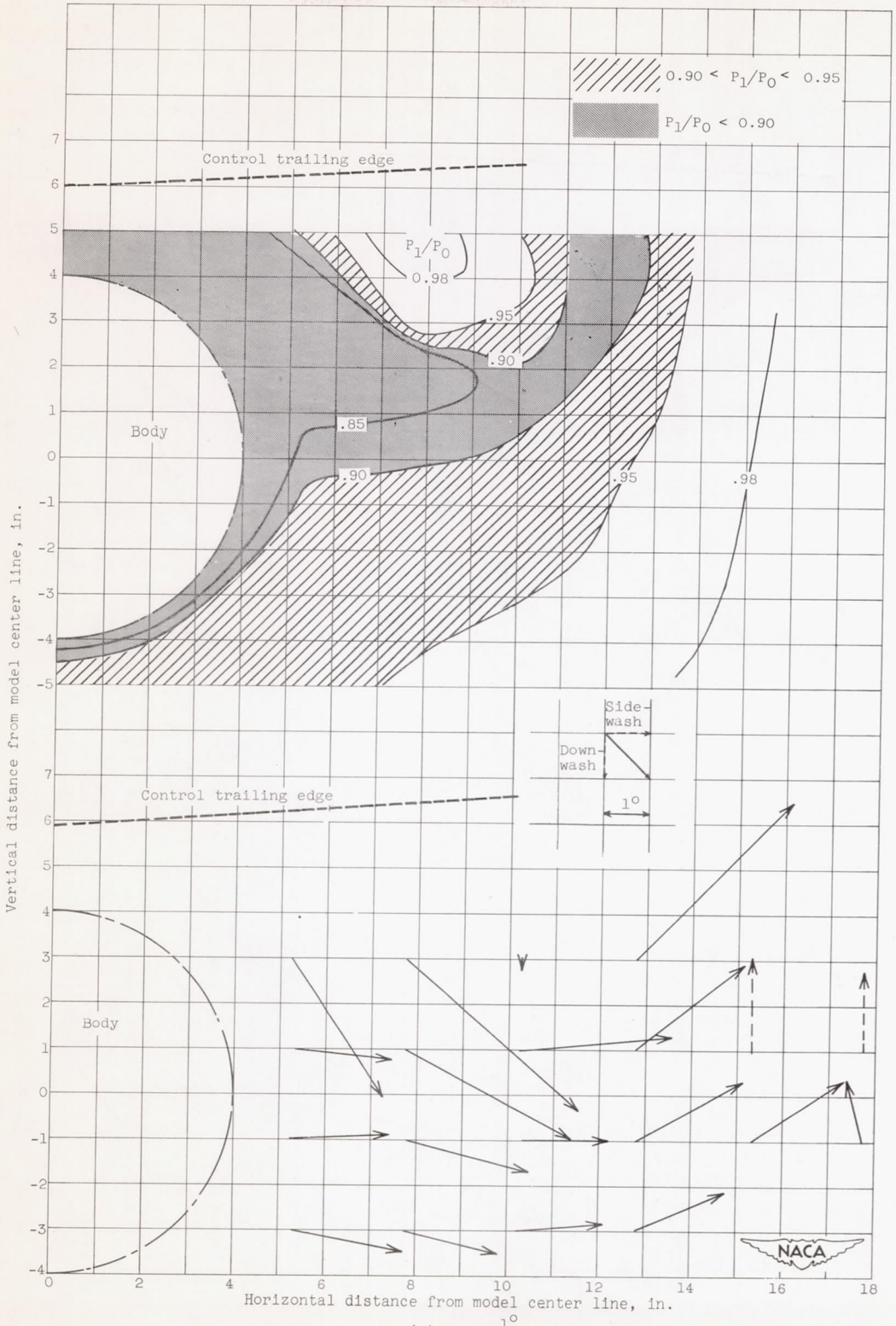

(d) $\delta_c = 9\frac{1}{2}^\circ$.

Figure 10. - Concluded. Total-pressure-ratio contours and flow-deflection angles of flow for body with control surface. Angle of attack, 6°.